SiliconPV 2023, 13th International Conference on Crystalline Silicon Photovoltaics
Carrier Selective Contacts, Metallization and Contact Formation
https://doi.org/10.52825/siliconpv.v1i.838

Published: 22 Feb. 2024

# Plasma-Assisted $N_2O$ Oxidation (PANO) in an Industrial Direct Plasma Reactor for TOPCon Production

Mathias Bories[1][https://orcid.org/0000-0002-4960-4062], Jana-Isabelle Polzin[1][https://orcid.org/0000-0002-2372-164X], Bernd Steinhauser[1][https://orcid.org/ 0000-0002-8689-9680], Martin Bivour[1], Jan Benick[1][https://orcid.org/1111-2222-3333-4444], Martin Hermle[1][https://orcid.org/0000-0002-2412-1734], and Stefan Glunz[1][https://orcid.org/ 0000-0002-9877-2097]

[1]Fraunhofer Institute for Solar Energy Systems ISE, Germany

**Abstract.** Plasma-Enhanced Chemical Vapor Deposition (PECVD) is an attractive tool for TOPCon production, as it enables uniformly *in situ* doped amorphous silicon (a-Si) and dielectric layer depositions with high throughput. However, a lean process requires *in situ* interfacial oxide growth in the same tool. In this work, we use Plasma-Assisted $N_2O$ Oxidation (PANO) in an industrial kHz direct plasma reactor (centrotherm c.PLASMA) to grow the oxide and deposit *in situ* phosphorus doped a-Si(n) as well as $SiN_x$ on asymmetric lifetime samples. Before optimization, the oxide thickness is non uniform on the wafer, and we show that it correlates with the passivation, the contact resistivity, and the doping profile in n-type TOPCon test structures. The passivation seems to benefit more from moderate in-diffusion in the case with PANO than in the case with thermal oxidation. This is probably due to enhanced field-effect passivation compensating for lower chemical passivation, which likely results from plasma-induced damage. After studying the influence of PANO process parameters on the oxide thickness and uniformity, we optimize them to obtain a non-uniformity as low as ±2% and a recombination current density down to 2.3 fA/cm² on planar wafers.

**Keywords:** In Situ Oxidation, Pecvd, Topcon, Doping Profile, Field-Effect Passivation

## 1. Introduction

While the high performance of TOPCon has been proven in the lab, motivating their transfer to the industry, there is still a lively debate about which process route is best suited for upscaling this technology. Due to its high deposition rate of *in situ* doped a-Si layers, PECVD could replace the mainly used Low-Pressure Chemical Vapor Deposition (LPCVD). To further simplify the process however, the interfacial oxide should be prepared in the same PECVD tool instead of using a wet chemical or thermal oxidation before a-Si deposition. Plasma-Assisted $N_2O$ Oxidation (PANO) further allows the incorporation of nitrogen to reduce the diffusion of boron, which could improve the passivation in p-type TOPCon [1]. While impressive results for both n-type ($J_{0s}$ = 2 fA/cm², $\rho_c$ = 4.2 mΩ.cm² [2]) and p-type TOPCon ($J_{0s}$ = 18.5 fA/cm², $\rho_c$ = 4.3 mΩ.cm² [3]) have already been shown using 13.56 MHz or microwave excitation of the plasma, the implementation of PANO in a kHz direct plasma reactor, which is commonly used for dielectric layer deposition in the industry and was proven to deposit high quality a-Si layers [4], would allow to use the same reactor for all layers without the need for additional high frequency sources.

In this contribution, we show that a high-quality PANO $SiO_x$ can be prepared in such a kHz direct plasma reactor where the main challenge is to control the oxide thickness and uniformity, as they have a great impact on the passivation and contact resistivity. After discussing this

correlation in consideration of the doping profiles, we show that the passivation difference between PANO and thermal oxidation-based n-TOPCon may be linked to plasma damage. Finally, we show how the oxidation parameters can be chosen to optimize the oxide thickness and uniformity, paving the way to its integration in TOPCon solar cells.

# 2. Impact of oxide thickness on passivation and contact resistivity

## 2.1. Experimental Layout

Asymmetric lifetime test samples were prepared on 200 µm-thick, 1 Ω.cm, n-type FZ wafers after standard RCA cleaning. Thermal oxidation was followed by *in situ* P-doped PECVD a-Si(n) deposition on the rear side to prepare a uniform reference n-TOPCon rear side. The front side thermal oxide was then removed in HF before growth of the PANO $SiO_x$ on the front side, with $N_2O$ as oxygen source. Its thickness was mapped using spectral ellipsometry (SE) before a-Si(n) deposition on the front side and subsequent annealing at 900°C under $N_2$, resulting in polycrystalline silicon (poly-Si) on both sides. The passivation was measured using Quasi-Steady-State Photoconductance (QSSPC) and modulated photoluminescence (Mod-PL) calibrated photoluminescence imaging (PLI) measurement after annealing and after hydrogenation with $SiN_x$. The $SiN_x$ layer was then removed in HF before Electrochemical Capacitance Voltage (ECV) measurement of the doping profile at different positions. Asymmetric vertical *I-V* test structures were finally prepared by evaporation of 2x2 cm² Ag/Ti windows on the front side (with PANO $SiO_x$) and 1 µm-thick Ag layer on the back side (with thermal $SiO_x$) to measure the contact resistivity.

Additionally, symmetric reference samples with standard n-TOPCon based on thermal $SiO_x$ on both sides were prepared and characterized to determine the contribution of the rear side of the asymmetric samples to the recombination current density and contact resistivity.

## 2.2. Experimental Results

The PANO $SiO_x$ grown in a kHz direct plasma reactor shows before process optimization a non-uniform thickness with a rotational symmetry over the wafer where the oxide is thinner in the centre and gets thicker towards the edge (see Figure 1. a). The passivation shows the same symmetry as the oxide thickness and the best passivation is achieved on a ring with intermediate thickness (see Figure 1. b).

By mapping the $SiO_x$ thickness and the i$V_{oc}$ on the same wafer (see Figure 2), we can study the interplay between oxide thickness and passivation at higher thickness resolution compared to a previous study [1]. We show that i$V_{oc}$ increases first with increasing oxide thickness, probably due to reduced dopant in-diffusion in the wafer and improved thermal stability, as previously reported for thermal oxides [5]. This can be seen on Figure 3, where the thinnest oxide results in a very deep dopant in-diffusion. However, when the oxide exceeds a thickness of around 1.3 nm, dopants are readily blocked from diffusion into to the c-Si bulk (see Figure 3) resulting in a reduced shielding of minority charge carriers and thus field-effect passivation [6]. After hydrogenation, this dependency of the passivation on oxide thickness above 1.3 nm is much less pronounced, indicating an improvement of the chemical passivation of the $SiO_x$/c-Si interface.

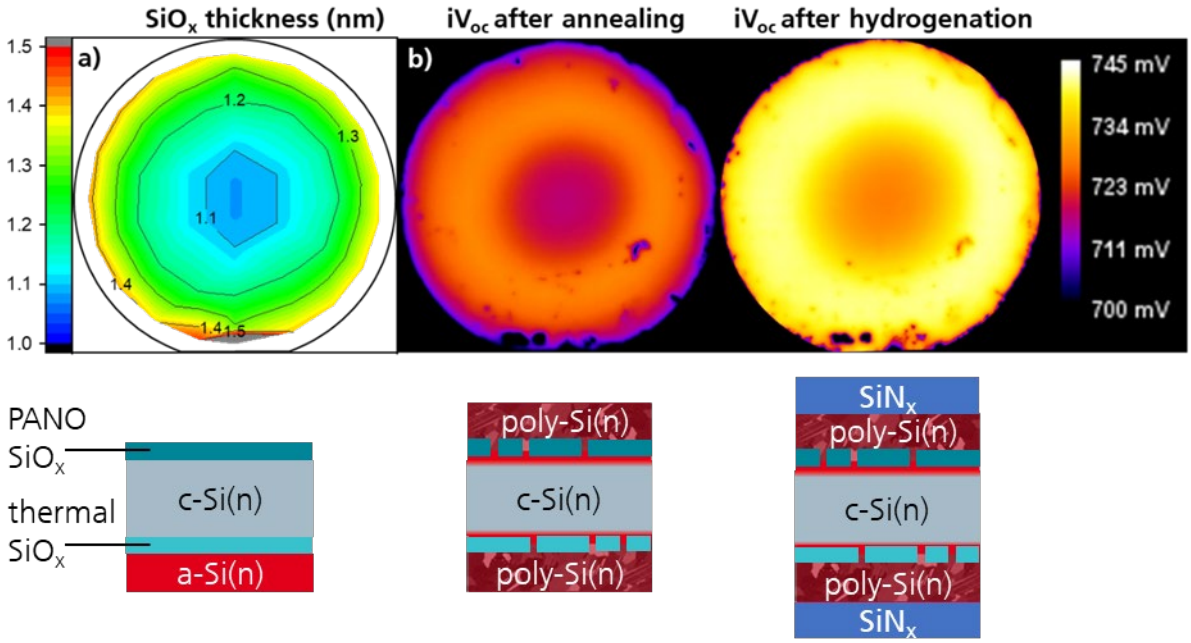


**Figure 1.** a) SE mapping of the oxide thickness before a-Si deposition and cross section of the sample structure. b) i$V_{oc}$ mappings from Mod-PL calibrated PLI of the asymmetric lifetime samples after annealing on the left and after hydrogenation with $SiN_x$ on the right and cross section of the sample structure.

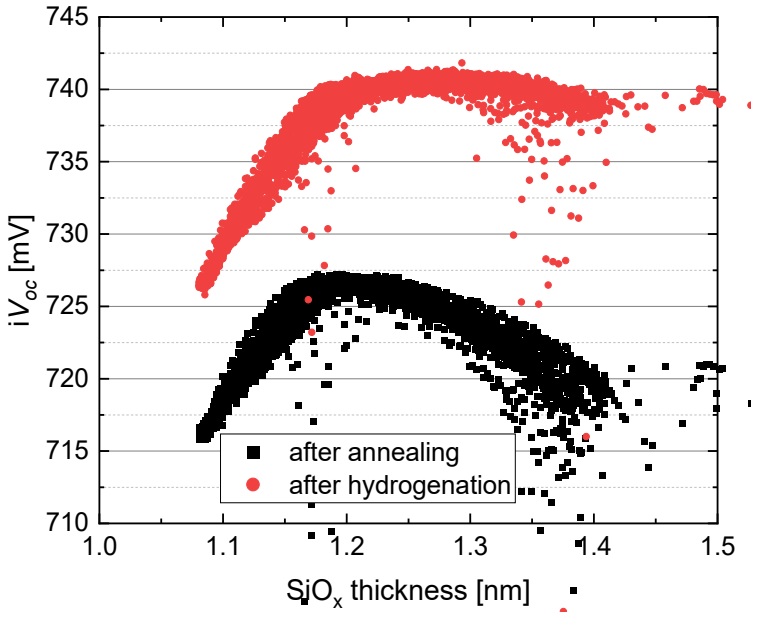


**Figure 2.** i$V_{oc}$ against oxide thickness at the same coordinates on the wafer, measured before and after hydrogenation with $SiN_x$

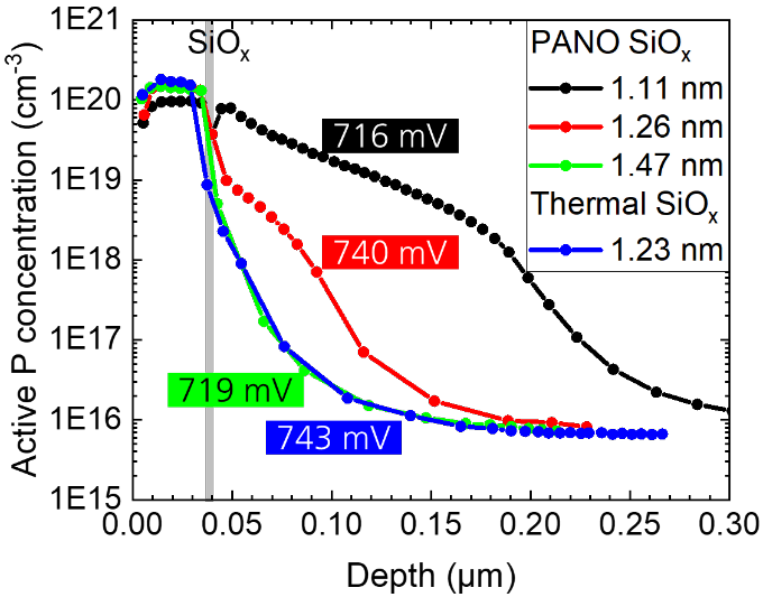


**Figure 3.** ECV measurements of active dopant profiles, corresponding $SiO_x$ thickness and i$V_{oc}$ after $SiN_x$.

As can be seen in the ECV doping profile measurements taken at different positions over the wafer (see Figure 3), the in-diffusion of P through the PANO $SiO_x$ strongly depends on the oxide thickness. Concentrations of electrically active P above $10^{18}$ $cm^{-3}$ have been measured down to 150 nm inside the c-Si wafer where the oxide was the thinnest and only down to 14 nm where the oxide was the thickest. The PANO $SiO_x$ of intermediate thickness leads to deeper in-diffusion than the thermal $SiO_x$ with comparable thickness, which hints at a lower thermal stability or weaker diffusion barrier provided by the PANO $SiO_x$. Interestingly the reference thermal $SiO_x$ results in a quite similar doping profile as the thickest PANO $SiO_x$ but a much better passivation, with i$V_{oc}$ = 743 mV after hydrogenation for the thermal $SiO_x$ and only 719 mV for the PANO $SiO_x$. This indicates that the thermally grown interfacial oxide gives a better chemical passivation. In contrast, the passivating contact with PANO $SiO_x$ seems to require more dopant in-diffusion to reach a similar passivation as with the thermal $SiO_x$, achieving a maximum i$V_{oc}$ of 740 mV after hydrogenation for an intermediate thickness of 1.26 nm, but too much in-diffusion leads to a degradation of the passivation, with i$V_{oc}$ decreasing to 716 mV.

Concerning the contact resistivity, an abrupt increase for an oxide thickness above around 1.4 nm (see Figure 4) probably results from the reduced dopant in-diffusion shown in Figure 3, together with reduced pinhole density and tunneling probability [7].

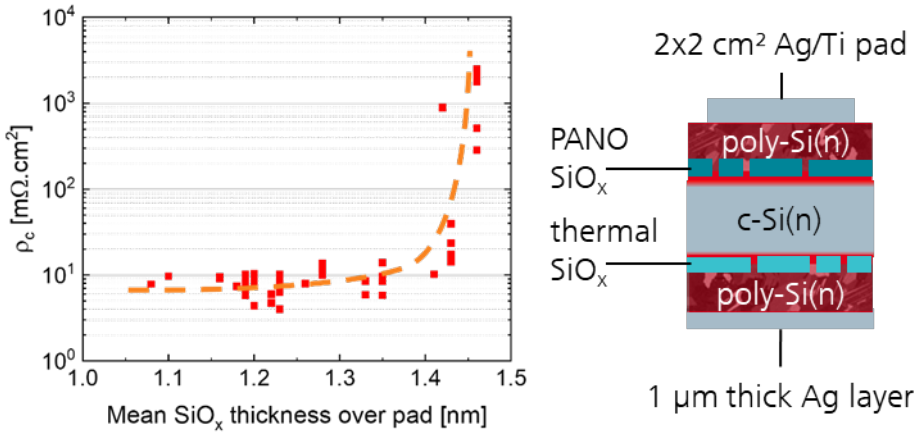


**Figure 4.** Contact resistivity measured on asymmetric vertical *I-V* samples, against $SiO_x$ thickness averaged over 2x2 cm² Ag/Ti window (dashed line is a guide to the eye)

## 3. Characterization of possible plasma damage

In order to characterize plasma-induced defect formation occurring during the PANO process, specific test structures were prepared by exposing RCA cleaned wafers to PANO processes with high or low RF power, subsequent removal of the oxide in HF and re-passivation with Atomic Layer Deposition (ALD) of aluminum oxide ($AlO_x$) and Forming Gas Anneal (FGA). Their injection dependent effective lifetime was measured with QSSPC and compared to reference samples that were not exposed to any PANO process and only had the oxide from RCA cleaning removed before $AlO_x$ deposition and FGA. As can be seen in Figure 5, the effective lifetime of the samples exposed to PANO processes reaches only around 1.8 ms at an excess carrier density of $10^{15}$ $cm^{-3}$ after passivation with $AlO_x$ and FGA, while the reference reaches 8.3 ms. This difference hints at possible plasma damage occurring during the PANO process that may explain the limited chemical passivation provided by the PANO $SiO_x$ shown in the previous part.

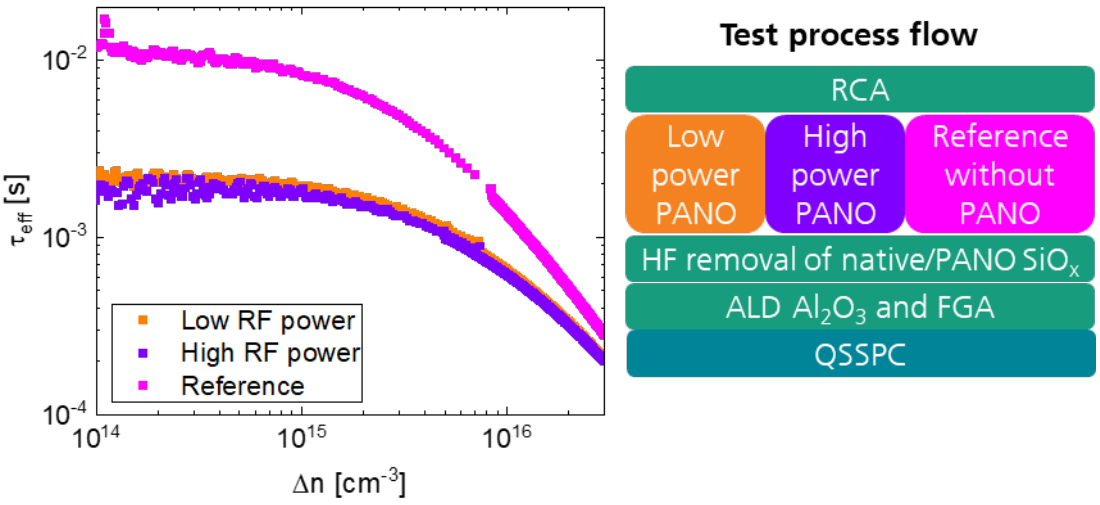


**Figure 5.** Effective lifetime of plasma damage test samples exposed to PANO processes with varied RF power and reference sample, measured after ALD $AlO_x$ and FGA and corresponding process flow.

## 4. Optimization of the oxide thickness and uniformity

Because of the strong impact of the PANO thickness on the passivation, it is necessary to achieve a good thickness uniformity on the wafer and wafer-to-wafer. The impact of the main oxidation parameters on oxide growth and uniformity is shown in Figure 6. For instance, increasing the radio frequency power $P_{RF}$ and partly replacing $H_2$ with Ar as buffer gas for $N_2O$ dilution improves the uniformity but strongly increases the oxide thickness. Thus, the oxidation time $t$ or RF pulse duration ($t_{on}$) needs to be reduced, or the duration between pulses ($t_{off}$) increased, to reach the optimal thickness.

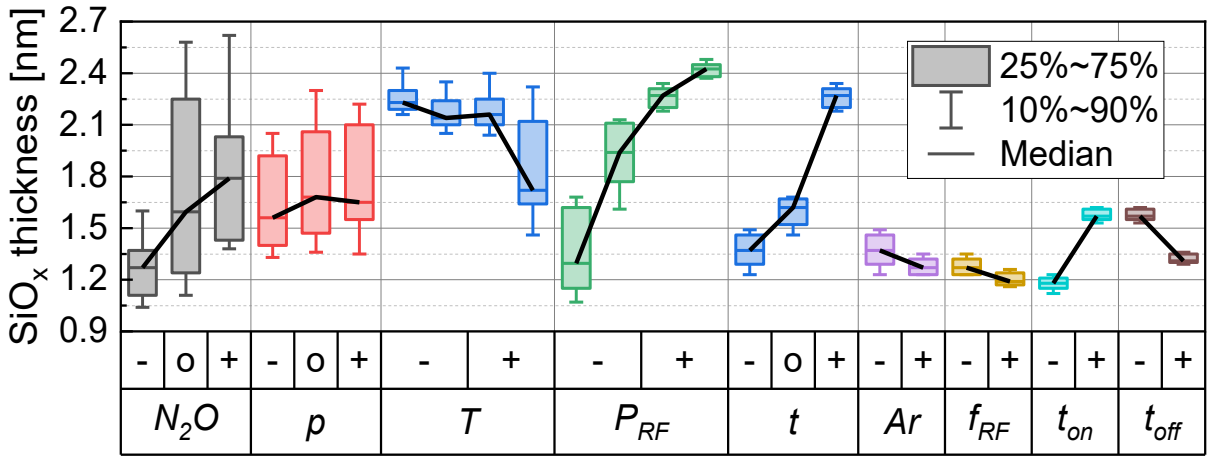


**Figure 6.** Impact of PANO parameters (Nitrous oxide flow $N_2O$, oxidation pressure $p$, temperature $T$, RF Power $P_{RF}$, process duration $t$, argon buffer flow $Ar$, RF frequency $f_{RF}$, RF pulse duration $t_{on}$ and duration between pulses $t_{off}$) on oxide thickness and uniformity

High thickness uniformity has been achieved by optimization of the PANO process parameters, leading to a non-uniformity as low as ±2%, similar to reference with thermal $SiO_x$. At the same time, recombination current densities $J_{0s}$ down to 2.4 fA/cm² and 6.5 fA/cm² were obtained after hydrogenation on planar and textured wafers, respectively, while the reference with thermal oxide reached 1.2 fA/cm² on planar wafers and 5 fA/cm² on textured wafers (see Figure 7).

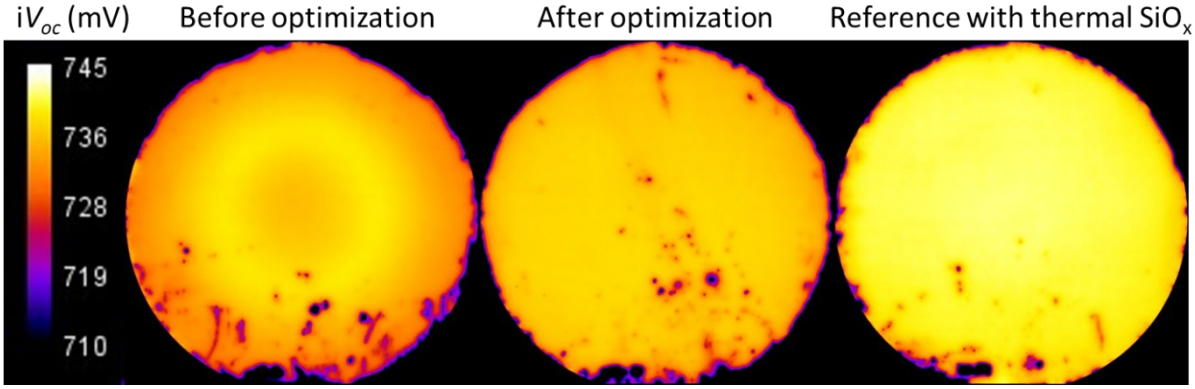


**Figure 7.** i$V_{oc}$ images of planar asymmetric lifetime samples before and after optimization of the PANO process, as well as symmetric reference sample with thermal $SiO_x$

## 5. Conclusion

The passivation provided by n-TOPCon with the PANO $SiO_x$ reaches a maximum for an optimal oxide thickness of about 1.2 to 1.3 nm, which is similar to the optimized thermal oxide. However, the optimized PANO $SiO_x$ shows more dopant in-diffusion than its thermal counterpart. Further research will focus here on the pinhole formation and microstructural composition

of the oxides. Low contact resistivities were obtained for an oxide thickness up to about 1.4 nm with PANO, limiting the working range for solar cells to a narrow thickness window. Finally, careful optimization of the PANO parameters improved the uniformity and passivation in n-TOPCon, with $J_{0s}$ as low as 2.4 fA/cm² and 6.5 fA/cm² on planar and textured wafers, respectively. This is comparable to our reference with thermal oxidation and shows the potential of the PANO process with regards to its implementation into TOPCon-based Si solar cells.

## Data availability statement

The data supporting the results of this contribution may be obtained from the authors upon reasonable request.

## Author contributions

Mathias Bories: Conceptualization, Methodology, Investigation, Data Curation, Writing - Original Draft, Visualization. Jana-Isabelle Polzin: Conceptualization, Supervision, Writing – review & editing. Bernd Steinhauser: Conceptualization, Resources. Martin Bivour: Supervision. Jan Benick: Conceptualization, Supervision, Writing – review & editing. Martin Hermle: Funding acquisition, Supervision, Writing – review & editing. Stefan Glunz: Conceptualization, Supervision, Writing – review & editing.

## Competing interests

The authors declare no competing interests.

## Funding

This work was supported by the German Federal Ministry for Economic Affairs and Climate Action BMWK and by the industry partners within the research project “PlasCon” under contract no. 03EE1137A

## Acknowledgement

The authors would like to thank A. Leimenstoll, F. Schätzle, R. Neubauer, E. M. Paul, and I. Koc for sample preparation and characterization.

## References

1. S. W. Glunz, B. Steinhauser, J.-I. Polzin, et al. "Silicon-based passivating contacts: The TOPCon route", Prog. Photovolt. Res. Appl. vol. 31, no. 4, pp. 341-359, 2023, doi: https://doi.org/10.1002/pip.3522
2. Y. Huang, et al. "Ultrathin silicon oxide prepared by in-line plasma-assisted $N_2O$ oxidation (PANO) and the application for n-type polysilicon passivated contact." Solar Energy Materials and Solar Cells, vol. 208, pp. 110389, 2020, doi: https://doi.org/10.1016/j.solmat.2019.110389
3. X. Guo, et al. "Comparison of different types of interfacial oxides on hole-selective p+-poly-Si passivated contacts for high-efficiency c-Si solar cells." Solar Energy Materials and Solar Cells, vol. 210, pp. 110487, 2020, doi: https://doi.org/10.1016/j.solmat.2020.110487

4. B. Steinhauser, et al. "Excellent surface passivation quality on crystalline silicon using industrial-scale direct-plasma TOPCon deposition technology." Solar RRL vol. 2, pp. 1800068, 2018, doi: https://doi.org/10.1002/solr.201800068
5. J.-I. Polzin, et al. "Temperature-induced stoichiometric changes in thermally grown interfacial oxide in tunnel-oxide passivating contacts." Solar Energy Materials and Solar Cells, vol. 218, pp. 110713, 2020, doi: https://doi.org/10.1016/j.solmat.2020.110713
6. G. Yang, et al. "Will $SiO_x$-pinholes for $SiO_x$/poly-Si passivating contact enhance the passivation quality?" Solar Energy Materials and Solar Cells, vol. 252, pp. 112200, 2023, doi: https://doi.org/10.1016/j.solmat.2023.112200
7. F. Feldmann, et al. "Charge carrier transport mechanisms of passivating contacts studied by temperature-dependent JV measurements." Solar Energy Materials and Solar Cells vol. 178, pp. 15-19, 2018, doi: https://doi.org/10.1016/j.solmat.2018.01.008